Vol. 23 • No. 19 • May 17 • 2011

D10488

www.advmat.de

ADVANCED MATERIALS

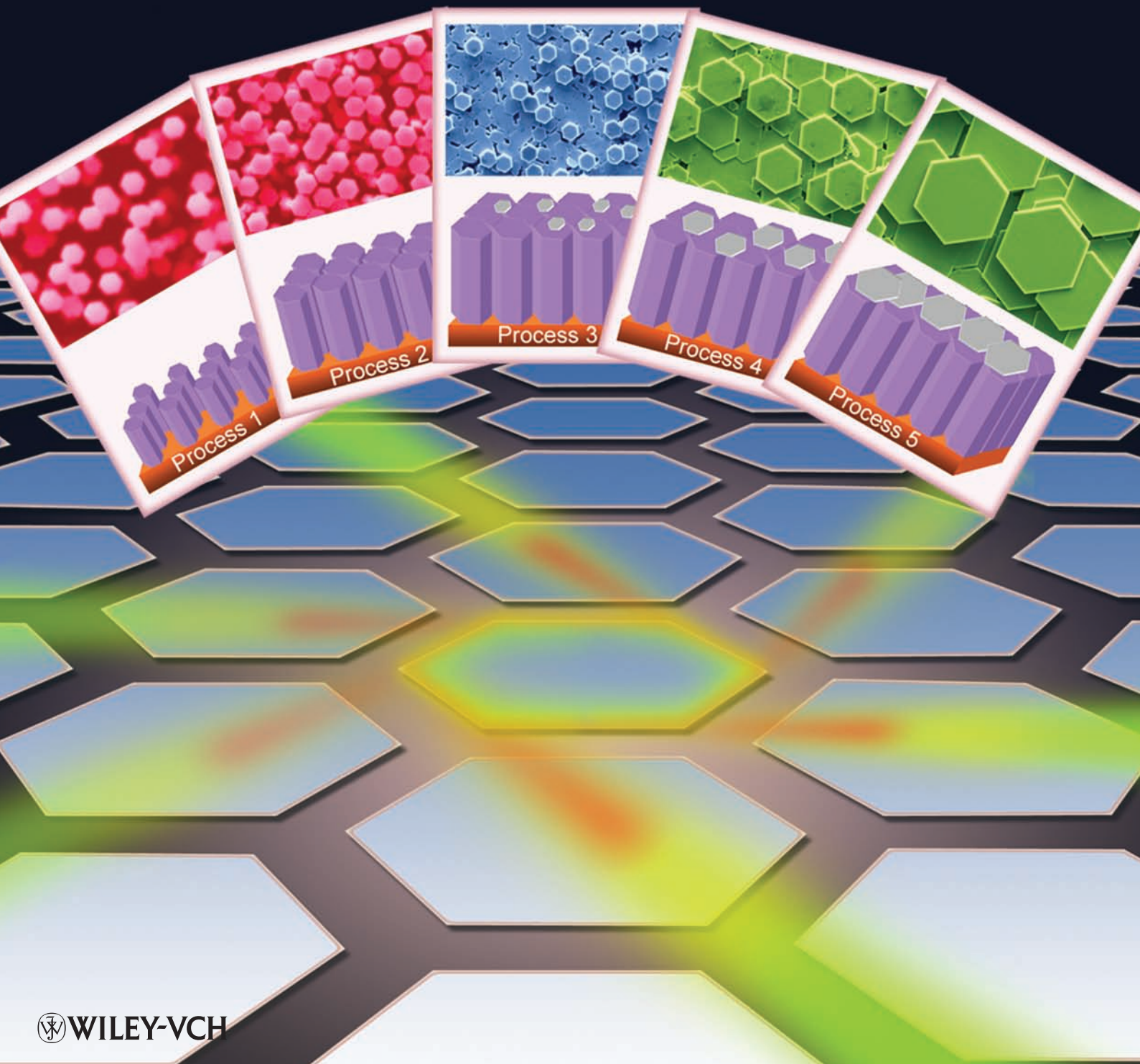

WILEY-VCH

Room Temperature Excitonic Whispering Gallery Mode Lasing from High-Quality Hexagonal ZnO Microdisks

Rui Chen, Bo Ling, Xiao Wei Sun, and Han Dong Sun**

In recent years, low-dimensional semiconductor structures have attracted extensive research interest because of their fundamental importance and wide range of potential applications in nanotechnology. Notable achievements have been witnessed by light-emitting devices, lasers, and solar cells based on group IV elements (Si and Ge),[1] and group III–V (GaN and GaAs),[2] and II–VI compound semiconductors (ZnO, ZnS, and CdSe).[3–6] Compared with other semiconductors, ZnO possesses a wide bandgap (≈3.37 eV) and large exciton binding energy (≈60 meV) at room temperature, which enables more efficient excitonic emission at higher temperatures.[7,8] Therefore, ZnO nanomaterials are recognized as potential building blocks for nanometer-scale electronic and optoelectronic devices operated in the blue and UV spectral regions.[9] In particular, the richness of nanostructures of ZnO facilitates the realization of various interesting optical confinement and laser cavities.

Several kinds of optical microcavities such as the Fabry–Pérot (F-P) cavity, photonic crystals, as well as whispering gallery modes (WGMs) have been involved in microlaser systems.[10] Among them, the WGM is of current interest because of the intrinsically high quality (*Q*) factor, low lasing threshold, and relatively simple fabrication.[11,12] However, most of the reports utilize a top-down synthetic approach which requires numerous fabrication steps and introduces more losses at the boundary.[13] In contrast, a bottom-up approach shows inherent advantages such as high material quality and high-throughput assembly.[14] It is noted that most of the ZnO nanostructures (such as nanowires, nanorails, and nanorods) have a perfectly hexagonally shaped cross-section, and the resonant effects in them have been investigated by cathodoluminescence and low temperature photoluminescence.[15–19] On the other hand, up till now, the study of room temperature resonance phenomena in larger disks has not been reported, although ZnO microdisks with diameters in the range of ≈10 μm can be readily obtained.[20] A detailed investigation of the WGM lasing properties from ZnO microdisks is needed to appreciate their possible applications.

In this study, high quality ZnO microdisks were obtained by a vapor phase transport (VPT) growth technique. It is found that the ZnO microdisks have a perfect hexagonal shape with various sizes, which allows for the investigation of the cavity length dependence of WGM. By using a micro-photoluminescence (μ-PL) system, we observed at room temperature very sharp WGM lasing modes from the ZnO disks at moderate excitation density, and the lasing mechanism originates from an excitonic effect, namely exciton–exciton scattering. Size-dependent investigation of the WGM lasing characteristics is carried out systematically. Furthermore, a sensing application based on WGM lasing in ZnO disks is proposed and demonstrated.

Figure 1 depicts a schematic diagram for the growth processes of ZnO microdisks, together with the corresponding plain-view scanning electron microscopy (SEM) images. Five different steps can be readily found during the growth. At the very beginning, hexagonal cross-section ZnO nanowires are grown vertically on the sapphire substrate. With the increase of the growth time, the length and density of the ZnO nanowires increase, leading to a film-like ZnO formed on top of the vertically aligned nanowires.[21] The transformation from 1D nanowires to a 2D film is similar to the characteristic of epitaxial lateral overgrowth, which has been found for material growth of GaN and ZnO.[22,23] From process 3 onward, ZnO disks can be found on top of the film-like surface, the size of which can be controlled by changing the growth parameters, such as temperature and reactor pressure. The enlarged disk size is attributed to the coalescence of grains originating from each disk in the initial stage. It is interesting to note that the perfect hexagonal shape of the ZnO disks exhibits an orientation identical to that of the bottom ZnO nanowires, indicating high crystalline quality of a single domain. The diameter of the ZnO disks is found to vary over a large range from ≈2 up to ≈14 μm, which enables us to explore the lasing properties of individual disks of different sizes.

The optical properties of an individual ZnO microdisk were investigated with a μ-PL system, and the experimental setup is shown schematically in **Figure 2**. The excitation laser was focused to a spot of 1.5 mm in diameter at a grazing angle ≈45° normal to the ZnO disk. The sample was placed on a sample holder mounted on an *X*-*Y*-*Z* movable stage. The signal emitted from an individual disk was collected with a UV objective and delivered to a camera for imaging, or focused into an optical fiber and directed into a 750 mm monochromator combined

R. Chen, Prof. H. D. Sun
Division of Physics and Applied Physics
School of Physical and Mathematical Sciences
Nanyang Technological University
637371, Singapore
E-mail: hdsun@ntu.edu.sg
B. Ling, Prof. X. W. Sun
Division of Microelectronics
School of Electrical and Electronics Engineering
Nanyang Technological University
639798, Singapore
E-mail: exwsun@ntu.edu.sg
Prof. X. W. Sun
Department of Applied Physics
College of Science
Tianjin University
Tianjin 300072, P. R. China

DOI: 10.1002/adma.201100423

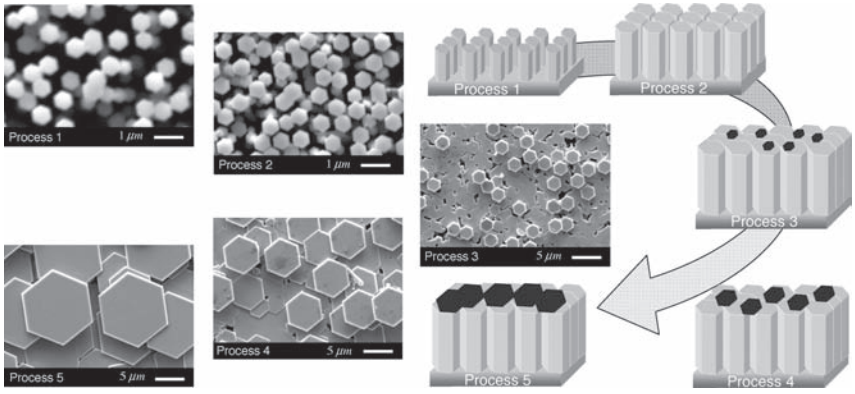

Figure 1. The growth process of ZnO microdisks. Process 1: vertically aligned ZnO nanowires grow on top of the substrate. Process 2: the transformation from 1D nanowires to a 2D film-like state. Process 3: ZnO disks exist on the top of the film-like surface. Processes 4 and 5: the growth of larger ZnO disks.

with a UV-enhanced back-illuminated charged coupled device (CCD) for spectral recording. A typical μ-PL spectrum of an individual ZnO disk (diameter = 12.56 μm) is shown in **Figure 3**. The optical images of the disk without and with optical excitation are shown in Figure 3c and d, respectively. It can be seen clearly that the disk has a perfect hexagonal shape and the trace lines of the disk boundaries are regularly arrayed with rotation angles of 60°, which confirms the lateral overgrowth and implies a high quality of the ZnO disk. It is also interesting to note that a violet pattern can be found on the surface under optical excitation, which will be discussed later.

Figure 3a shows the power-dependent μ-PL spectra of a ZnO disk at room temperature. Under low excitation, such as 0.06 MW cm^{-2}, the spectrum displays a weak spontaneous emission from ZnO. As the excitation density increases, sharp peaks located at ≈390 nm emerge from the emission spectrum, the intensity of which increase rapidly with a further increase of excitation density. A plot of integrated PL intensity of the peaks with excitation density is shown in the inset of Figure 3a. Such a non-linear increase of the emission intensity indicates a lasing phenomenon in the ZnO disk. The lasing threshold is found to be ≈0.28 MW cm^{-2}, which is comparable to those obtained at low temperature.[12]

In order to understand the lasing mechanism, a μ-PL spectrum under low excitation density is enlarged and plotted in Figure 3b. At a low pumping intensity, a spontaneous emission peak located at ≈380 nm (3.2632 eV) is observed, which can be attributed to the recombination of a free exciton (FX).[24] At higher excitation density, the FX becomes saturated and

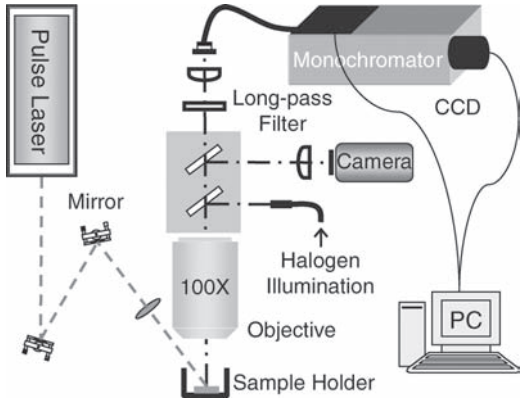

Figure 2. Schematic setup for μ-PL investigation of an ZnO disk.

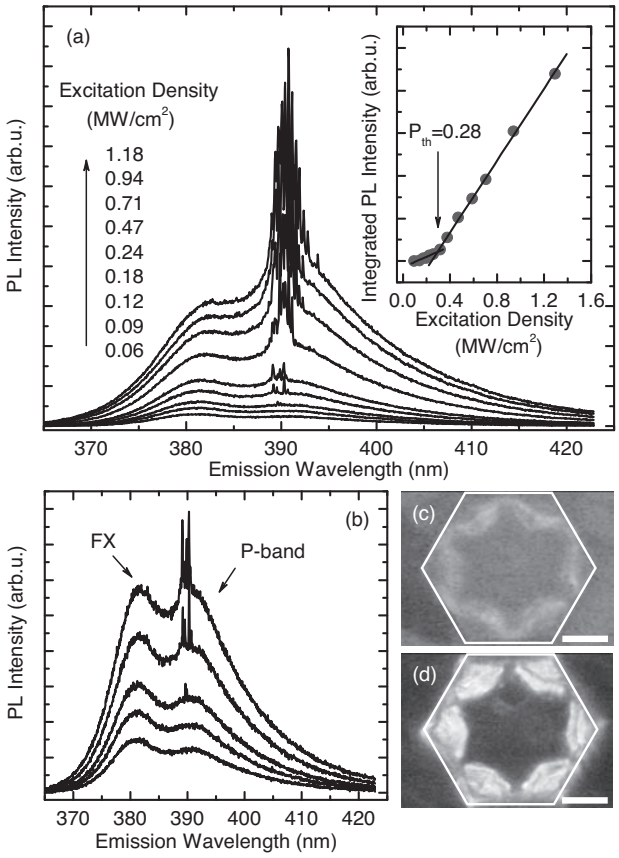

Figure 3. a) The μ-PL spectrum of an individual ZnO disk under different excitation density. The inset shows the dependence of integrated PL intensity on the excitation density. b) The enlarged part of the μ-PL spectrum under low excitation density (from 0.06–0.24 MW cm^{-2}). c,d) The optical images of the ZnO disk with halogen illumination and optical excitation, with a scale bar of 3 μm.

the emission at ≈390 nm (3.1795 eV) is more pronounced. It is known that inelastic exciton–exciton scattering may occur in two ways; namely, one of the excitons may be scattered into an excited state (P_n-band emission) or into a continuum state (P-band emission).[25] Under this situation, the energy of an emitted photon can be calculated by,[26]

$$E_n = E_{ex} - E_{ex}^b\left(1 - \frac{1}{n^2}\right) - \frac{3}{2}k_B T \quad (n = 2, 3, 4, ..., \infty) \qquad (1)$$

where E_{ex} is the energy of FX, E_{ex}^b is the exciton binding energy, n is the quantum number of the envelope function, and $k_B T$ is the thermal energy. The energy difference between the two bands is deduced to be 83.7 meV, which is close to the calculated value (85.8 meV). Therefore, the emission at ≈390 nm can be ascribed to the P-band emission of ZnO, which indicates excitonic lasing occurring from the disk. It should be mentioned that P-band lasing is different from electron–hole plasma lasing which has been observed before.[27] This is very important because it introduces a new emission mechanism with an even higher efficiency than FX recombination, which offers a very large optical gain and thus can be used for low-threshold lasers.

Lasing phenomena could not happen without appropriate cavity feedback. Various feedback mechanisms may account for the lasing, such as a random resonant effect, an F-P cavity, or WGM. In our experiment, since the lasing is observed from a single ZnO disk, it cannot be attributed to random lasing caused by multiple scattering in a disordered medium.[28,29] For an F-P cavity, it can be formed either by the hexagonal facets (**Figure 4**a) or by two opposing edge facets of the disk (Figure 4b). The hexagonal-shaped dielectric cavity can also support quasi-WGM (Figure 4c) and WGM (Figure 4d), where the light is totally reflected by the three (six) lateral sides of the ZnO microneedle with a 30° (60°) incident angle because the critical angle of total internal reflection is about 25.8° at the ZnO/air boundary.[30] The Q factor is an important parameter to describe a laser cavity. From the experiment, the Q factor is estimated to be as high as ≈3300 according to the definition $Q = \lambda/\Delta\lambda$, where λ is the peak wavelength and $\Delta\lambda$ is the linewidth of the peak, respectively.

The Q factor for a F-P cavity can be determined by the following equation[31]

$$Q = 2\pi nL/\lambda(1 - R) \qquad (2)$$

where $n \approx 2.3$ is the refractive index, R is the reflectivity at the ZnO/air boundary ($R \approx 15.5\%$), and L is the cavity length. For the case of FP-2, the deduced Q factor is only 468, which is far smaller than the experimentally observed value. Furthermore, the Q factor could be even smaller if other losses such as the scattering inside the cavity are considered. On the other hand, if the experimentally obtained Q factor was inserted into the equation, the cavity length is deduced to be 75.4 μm. Therefore, it is concluded that an F-P cavity provides a very low Q factor, which is absent in the ZnO microdisks.

Considering the case of a WGM, the Q factor for a m- faceted polygonal cavity can be expressed as:[32]

$$Q = \frac{\pi Dmn R^{m/4}}{2\lambda\left(1 - R^{m/2}\right)} \sin\left(\frac{2\pi}{m}\right) \qquad (3)$$

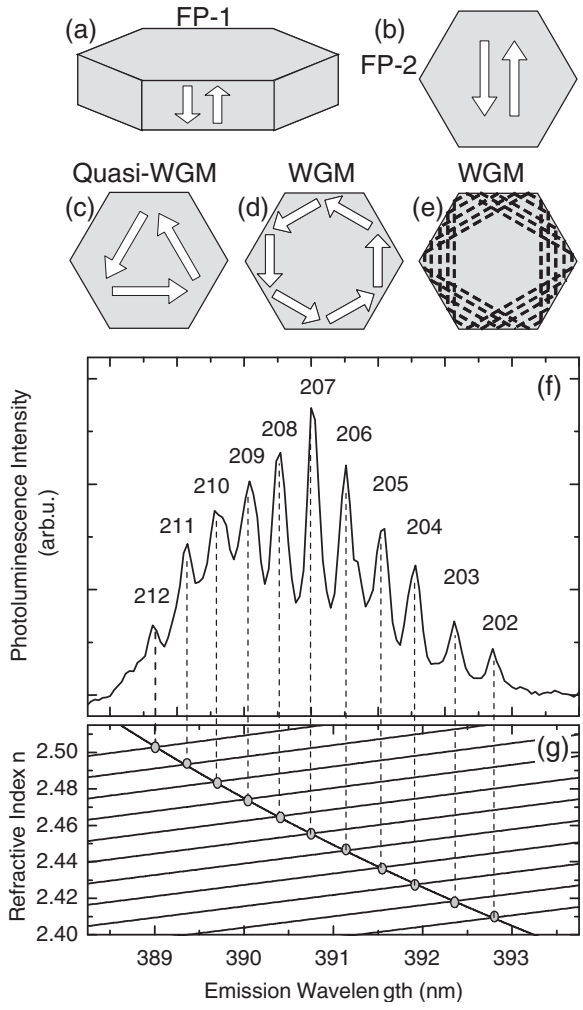

Figure 4. a–e) Schematics of possible resonant cavity modes in the ZnO disk. f) The lasing spectra of a ZnO disk with an excitation density of 1.18 MW cm^{-2}. g) The inverse functions of WGM modes with the corresponding mode numbers given in (f). The wavelengths are determined by the intersection points with the dispersion of the refractive index of ZnO based on Sellmeier's function.

where D is the diameter of the circle that circumscribes the polygon, m is the number of facets, and R is the reflectivity of the facets. If the laser was quasi-WGM or WGM, it can be deduced that the reflectivity is about 89.35% for a quasi-WGM cavity and 93.71% for a WGM cavity. This result is reasonable for the total internal reflectivity considering the cavity loss at the corners.[33] In fact, for a WGM cavity, the boundary does not have to be hit in the center between two corners, as depicted by the dashed line in Figure 4e.[12] This is why an intense optical field distributed at the corners of the hexagonal disk but with a very low intensity in the disk center is observed, as shown in Figure 3d. It is also notable that the WGM is more preferable because of a better optical confinement. So we ascribe the observed P-band excitonic lasing to WGM.

To understand the lasing observed in the ZnO disk clearly, an optical mode calculation was performed. The resonant

wavelength λ and the corresponding mode number N can be deduced through a classical plane-wave model for the WGM cavity,[34]

$$N = \frac{3\sqrt{3}nD}{2\lambda} - \frac{\pi}{6}\tan^{-1}\left(n\sqrt{3n^2-4}\right) \quad (4)$$

where the refractive index n for a transverse electric (TE) mode is described by the Sellmeier's dispersion function,[18,35]

$$n(\lambda) = \left(1 + \frac{2.4885\lambda^2}{\lambda^2 - 102.30^2} + \frac{0.2150\lambda^2}{\lambda^2 - 372.60^2} + \frac{0.2550\lambda^2}{\lambda^2 - 1850^2}\right)^{1/2} \quad (5)$$

It should be mentioned that the WGM lasing only occurs in the plane perpendicular to the c -axis of the ZnO disk. Although the measurement was performed along the c -axis of ZnO, the signal observed is actually the scattered emission from the boundaries of the ZnO disk. Therefore, only the TE mode is involved for discussion because of a much weaker intensity of transverse magnetic (TM) polarized emission in ZnO.[17] Based on the above equations, N can be determined for a series of TE modes. Once N was calculated, we inverted the function $N = f(n, \lambda)$ from Equation (4) into a linear function $n = f^{-1}(n, \lambda, N) = g(n, N)\lambda$. Finally, as shown in Figure 4g, when the dispersion curve of n is added, accurate values for the WGM peak wavelengths can be determined at the intersections of a series of solid lines for different N (from 202 to 212). Figure 4f shows the lasing spectrum excited at 1.18 MW cm^{-2}. It can be seen that the lasing emission peak positions match the theoretical modes very well, which confirms the WGM lasing phenomenon. From the best fit of the experimental data, a value for the diameter of 12.85 μm can be obtained, which is close to the size of the ZnO disk as shown in Figure 3d.

In order to obtain more information about the lasing characteristics from the WGM cavity, a size-dependent lasing measurement was carried out on individual ZnO microdisks at room temperature. **Figure 5**a–c present lasing spectra of ZnO microdisks with various diameters, while the insets show the dependence of the integrated PL intensity on excitation density, and the corresponding PL images of WGM lasing. Furthermore, the lasing threshold for different diameters of ZnO disks is summarized in Figure 5d. It is found that the lasing threshold decreases with the increase in diameter of the ZnO microdisks.[36] Previous studies show that the WGM lasing threshold strongly depends on Q and the confinement factor (Γ). A $1/D^2$ relationship is expected for disk diameter and lasing threshold, because the lasing threshold is inversely proportional to Q and Γ, respectively.[14] It is noted that the experimental data can be well fitted to a $1/D^2$ function, which further confirms the WGM lasing action in the ZnO disks. The increase of lasing threshold can be attributed to the smaller disk cavity volume, which provides less spatial overlap between the WGM and the ZnO gain medium, resulting in more light leakage (optical loss) from the WGM cavity. The interpretation is also supported by the differences in the PL images as shown in the insets of Figure 5. It can be seen that with the decrease of the diameter of the disk, the optical field distribution of the WGM lasing decreases, and finally, an intense optical field only distributes at the corners for a small ZnO disk.[14,37]

Based on the discussion above, it is noted that the threshold of the WGM lasing depends strongly on the surrounding

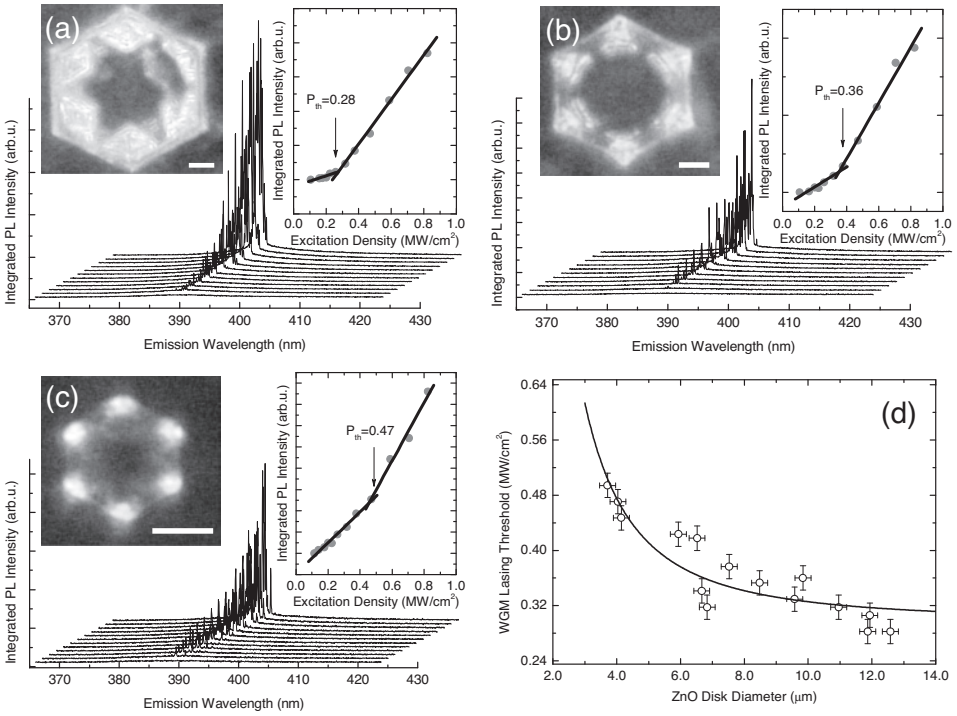

Figure 5. a–c) Room temperature WGM lasing spectra of ZnO disks with various diameters. PL images of the WGM lasing are shown with a scale bar of 2 μm. d) The room temperate WGM lasing threshold changes with the diameter of the ZnO disk. The curve is the best fit to a $1/D^2$ function.

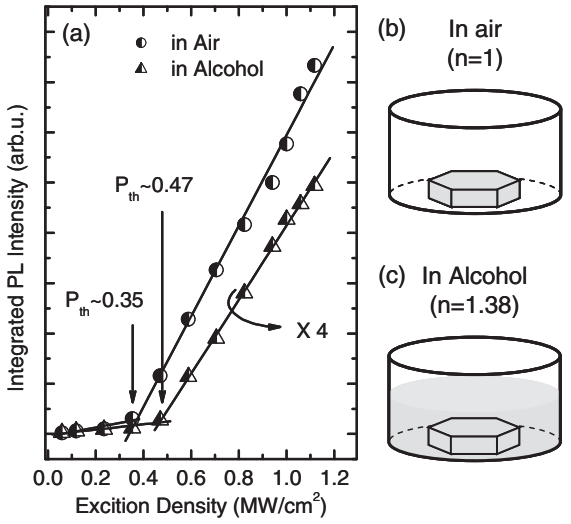

Figure 6. The integrated PL intensity of a ZnO disk in air and alcohol under different excitation densities. The data of WGM lasing from the ZnO disk in alcohol is multiplied by 4.

medium.[38] With the increase of the refractive index of the surrounding medium, reflectivity at the boundary between ZnO and the medium will decrease, which leads to a smaller Q and Γ factor, and results in a higher WGM lasing threshold. Here, a proof-of-concept sensing application based on ZnO WGM lasing is demonstrated. We record the lasing spectra of a ZnO disk in air and in alcohol, respectively. **Figure 6** plots the integrated PL intensity with the change of excitation density for two measurements, with the schematic diagrams showing the difference between two measurements. As expected, the WGM lasing threshold of ZnO in alcohol increases from 0.35 to 0.47 MW cm^{-2}, while the integrated PL intensity decreases more than four times. Our results indicate the high sensitivity of the WGM lasing in a ZnO disk, and research down this line may help to advance photonic sensing devices for label-free detection possibly down to molecule level.[39]

In summary, we experimentally demonstrated high quality hexagonal ZnO microdisks with diameters from ≈2 up to ≈14 μm fabricated by a VPT method. Under optical excitation at room temperature, P-band excitonic lasing is observed from individual ZnO disks. The analysis of the lasing characteristics indicates that only WGM can account for the observed emission. Theoretical and experimental investigations demonstrate that the lasing threshold is inversely proportional to the square of the ZnO disk diameter. In addition, the sensing application of WGM lasing is proposed and demonstrated. These findings provide detailed lasing characteristics of WGM from ZnO microdisks, which show promising applications for low threshold UV lasers and high sensitivity sensors.

Experimental Section

The ZnO disks used herein were grown on c-sapphire by a VPT method using Zn powder as the source material. First, a small quartz tube containing the source and the substrate was inserted into a horizontal quartz tube furnace. During the synthesis, the substrate temperature was kept at ≈450 °C and the gas pressure was kept at ≈2 torr under a constant flow of 100 sccm for Ar and 1 sccm for O_2, respectively. Further characterization was performed on a JEOL JSM-7001F field emission scanning electron microscope operating at 15 kV. The μ-PL measurement was carried out at room temperature with a pulsed Nd:YAG 4th harmonic (266 nm) laser as excitation source. The pulse width and repetition rate of the laser were 1 ns and 60 Hz, respectively.

Acknowlegements

Support from the Singapore Ministry of Education through the Academic Research Fund (Tier 1) under Project No. RG63/10 and from National Science Foundation of China (NSFC) (61006037 and 61076015) are gratefully acknowledged.

Received: February 2, 2011
Published online: April 4, 2011

[1] J. Xiang, W. Lu, Y. Hu, Y. Wu, H. Yan, C. M. Lieber, *Nature* **2006**, *441*, 489.
[2] R. Yan, D. Gargas, P. Yang, *Nat. Photonics* **2009**, *3*, 569.
[3] Z. K. Tang, G. K. L. Wong, P. Yu, M. Kawasaki, A. Ohtomo, H. Koinuma, Y. Segawa, *Appl. Phys. Lett.* **1998**, *72*, 3270.
[4] R. Chen, D. Li, B. Liu, Z. Peng, G. G. Gurzadyan, Q. Xiong, H. D. Sun, *Nano Lett.* **2010**, *10*, 4956.
[5] R. Chen, M. I. B. Utama, Z. Peng, B. Peng, Q. Xiong, H. D. Sun, *Adv. Mater.* **2011**, *23*, 1404.
[6] M. H. Huang, S. Mao, H. Feick, H. Q. Yan, Y. Y. Wu, H. Kind, E. Weber, R. Russo, P. D. Yang, *Science* **2001**, *292*, 1897.
[7] H. D. Sun, T. Makino, N. T. Tuan, Y. Segawa, M. Kawasaki, A. Ohtomo, K. Tamura, H. Koinuma, *Appl. Phys. Lett.* **2001**, *78*, 2464.
[8] H. D. Sun, Y. Segawa, M. Kawasaki, A. Ohtomo, K. Tamura, H. Koinuma, *J. Appl. Phys.* **2002**, *91*, 6457.
[9] W. Wang, C. J. Summers, Z. L. Wang, *Nano Lett.* **2004**, *4*, 423.
[10] K. J. Vahala, *Nature* **2003**, *424*, 839.
[11] A. C. Tamboli, E. D. Haberer, Rajat. Sharma, K. H. Lee, S. Nakamura, E. L. Hu, *Nat. Photonics* **2007**, *1*, 61.
[12] C. Czekalla, T. Nobis, A. Rahm, B. Cao, J. Zúñiga-Pérez, C. Sturm, R. Schmidt-Grund, M. Lorenz, M. Grundmann, *Phys. Status Solidi B* **2010**, *247*, 1282.
[13] S. L. McCall, A. F. J. Levi, R. E. Slusher, S. J. Pearton, R. A. Logan, *Appl. Phys. Lett.* **1992**, *60*, 289.
[14] D. J. Gargas, M. C. Moore, A. Ni, S.-W. Chang, Z. Zhang, S.-L. Chuang, P. Yang, *ACS Nano* **2010**, *4*, 3270.
[15] C. Kim, Y.-J. Kim, E.-S. Jang, G.-C. Yi, H. H. Kim, *Appl. Phys. Lett.* **2006**, *88*, 093104.
[16] J. Liu, Q. M. Ngo, K. H. Park, S. Kim, Y. H. Ahn, J.-Y. Park, K. H. Koh, S. Lee, *Appl. Phys. Lett.* **2009**, *95*, 221105.
[17] C. Czekalla, C. Sturm, R. Schmidt-Grund, B. Cao, M. Lorenz, M. Grundmann, *Appl. Phys. Lett.* **2008**, *92*, 241102.
[18] J. Liu, S. Lee, Y. H. Ahn, J.-Y. Park, K. H. Koh, K. H. Park, *Appl. Phys. Lett.* **2008**, *92*, 263102.
[19] H. Dong, L. Sun, W. Xie, W. Zhou, X. Shen, Z. Chen, *J. Phys. Chem. C* **2010**, *114*, 17369.
[20] C. X. Xu, X. W. Sun, Z. L. Dong, M. B. Yu, *Appl. Phys. Lett.* **2004**, *85*, 3878.
[21] D. C. Kim, J. H. Lee, H. K. Cho, J. H. Kim, J. Y. Lee, *Cryst. Growth Des.* **2010**, *10*, 321.
[22] D. Kapolnek, S. Keller, R. Vetury, R. D. Underwood, P. Kozodoy, S. P. Den Baars, U. K. Mishra, *Appl. Phys. Lett.* **1997**, *71*, 1204.
[23] J. J. Cole, X. Wang, R. J. Knuesel, H. O. Jacobs, *Nano Lett.* **2008**, *8*, 1477.

[24] R. Chen, Y. Q. Shen, F. Xiao, B. Liu, G. G. Gurzadyan, Z. L. Dong, X. W. Sun, H. D. Sun, *J. Phys. Chem. C* **2010**, *114*, 18081.
[25] H. D. Sun, T. Makino, N. T. Tuan, Y. Segawa, Z. K. Tang, G. K. L. Wong, M. Kawasaki, A. Ohtomo, K. Tamura, H. Koinuma, *Appl. Phys. Lett.* **2000**, *77*, 4250.
[26] C. F. Klingshirn, *Semiconductor Optics* Springer, Berlin **2007**.
[27] J. Dai, C. X. Xu, P. Wu, J. Y. Guo, Z. H. Li, Z. L. Shi, *Appl. Phys. Lett.* **2010**, *97*, 011101.
[28] H. Cao, Y. G. Zhao, S. T. Ho, E. W. Seelig, Q. H. Wang, R. P. H. Chang, *Phys. Rev. Lett.* **1999**, *82*, 2278.
[29] C. W. Cheng, B. Liu, H. Y. Yang, W. W. Zhou, L. Sun, R. Chen, S. F. Yu, J. X. Zhang, H. Gong, H. D. Sun, H. J. Fan, *ACS Nano* **2009**, *3*, 3069.
[30] V. V. Ursaki, A. Burlacu, E. V. Rusu, V. Postolake, I. M. Tiginyanu, *J. Opt. A-Pure Appl. Opt.* **2009**, *11*, 075001.
[31] R. Chen, H. D. Sun, T. Wang, K. N. Hui, H. W. Choi, *Appl. Phys. Lett.* **2010**, *96*, 241101.
[32] A. K. Bhowmik, *Appl. Opt.* **2000**, *39*, 3071.
[33] J. Wiersig, *Phys. Rev. A* **2003**, *67*, 023807.
[34] X.-G. Wei, J.-H. Wu, G.-X. Sun, Z. Shao, Z.-H. Kang, Y. Jiang, J.-Y. Gao, *Phys. Rev. A* **2005**, *72*, 023806.
[35] X. W. Sun, H. S. Kwok, *J. Appl. Phys.* **1999**, *86*, 408.
[36] J. Dai, C. X. Xu, K. Zheng, C. G. Lv, Y. P. Cui, *Appl. Phys. Lett.* **2009**, *95*, 241110.
[37] C. Zhang, F. Zhang, X. W. Sun, Y. Yang, J. Wang, J. Xu, *Opt. Lett.* **2009**, *34*, 3349.
[38] F. Vollmer, D. Braun, A. Libchaber, M. Khoshsima, I. Teraoka, S. Arnold, *Appl. Phys. Lett.* **2002**, *80*, 4057.
[39] F. Vollmer, S. Arnold, *Nat. Methods* **2008**, *5*, 591.